PRAMANA — journal of physics

Vol. 83, No. 4
October 2014
pp. 597–617

Coherent nonlinear electromagnetic response in twisted bilayer and few-layer graphene

VIPIN KUMAR*, ENAMULLAH, UPENDRA KUMAR and GIRISH S SETLUR

Department of Physics, Indian Institute of Technology Guwahati, Guwahati 781 039, India
*Corresponding author. E-mail: k.vipin@iitg.ernet.in

MS received 28 November 2013; revised 7 February 2014; accepted 11 February 2014
DOI: 10.1007/s12043-014-0808-4; ***e*Publication:** 27 September 2014

Abstract. The phenomenon of Rabi oscillations far from resonance is described in bilayer and few-layer graphene. These oscillations in the population and polarization at the Dirac point in n-layer graphene are seen in the nth harmonic term in the external driving frequency. The underlying reason behind these oscillations is attributable to the pseudospin degree of freedom possessed by all these systems. Conventional Rabi oscillations, which occur only near resonance, are seen in multiple harmonics in multilayer graphene. However, the experimentally measurable current density exhibits anomalous behaviour only in the first harmonic in all the graphene systems. A fully numerical solution of the optical Bloch equations is in complete agreement with the analytical results, thereby justifying the approximation schemes used in the latter. The same phenomena are also described in twisted bilayer graphene with and without an electric potential difference between the layers. It is found that the anomalous Rabi frequency is strongly dependent on twist angle for weak applied fields – a feature absent in single-layer graphene, whereas the conventional Rabi frequency is relatively independent of the twist angle.

Keywords. Graphene; bilayer graphene; multilayer graphene; non-linear phenomenon; Rabi oscillations.

PACS Nos 78.67.Wj; 78.67.Pt

1. Introduction

Graphene [1] is the newest 2D-layered nanostructured and carbon-based material that can even be as thin as the size of a single carbon atom. It consists of tightly packed flat carbon sheets in a two-dimensional plane. It is also the basic building block for graphitic materials of all other dimensionalities [2,3]. The most attractive features of graphene are its zero band gap, linear energy–momentum dispersion [3]: $\hat{H} = \hbar v_{\mathrm{F}} \boldsymbol{\sigma} \cdot \mathbf{k}$ and massless chiral quasiparticles band structure near the Dirac points. These quasiparticles follow relativistic Dirac–Weyl equation, where the velocity of light is replaced by the Fermi velocity, $v_{\mathrm{F}} \approx c/300$ of quasiparticles.

Subsequently, bilayer graphene (BLG), graphite with two graphene sheets, became a subject of intense study in its own right due to its gate tuneable band gap between the conduction and valance bands. It can be modelled as two coupled honeycomb lattices consisting of inequivalent lattice sites A1, B1 and A2, B2 in the bottom and top layers, respectively. These two layers are arranged according to Bernal (A1–B2) stacking [4–6]. In BLG, the massive chiral quasiparticles, showing Berry phase [4] of 2π, are charge carriers that exhibit parabolic dispersion near the Dirac points, where the valance band and conduction band touch one another. These chiral quasiparticles possess pseudospin degrees of freedom, which lie in the plane of the layers and turn twice as quickly as the direction of the momentum [4]. In practical BLG samples (especially, those produced by epitaxy), these two graphene layers are not exactly AB but, there is a relative twist between the layers. Twisting, also called stacking defect, is obviously absent in monolayer graphene. Twisted BLG's low-energy band structure is drastically different from the AB-stacked bilayer and possesses intriguing electronic properties. Unlike biased AB-stacked BLG [6], a potential difference between the twisted layers does not open a gap in the energy spectrum. Rather, this potential difference between the layers gives rise to a vertical shift in the energies at the degeneracy points [7]. The electronic band structure of twisted graphene bilayer has also been confirmed experimentally [8–10]. We wish to investigate what effect twisting has on a property we have been stressing is unique to graphene-based systems, i.e. anomalous Rabi oscillations (ARO) [11]. As expected, we find that the anomalous Rabi frequency (ARF) is highly sensitive to the low-energy band structure and therefore, depends strongly on the twist, whereas the conventional Rabi frequency (CRF), applicable near resonance, which occurs far from the bottom of the bands, is much less affected by the twist. Thus, AROs are useful barometers for studying the low-energy electronic structure of graphene-based systems. Unlike other methods, such as ARPES, which only confirm that the graphene dispersion is linear, ARO also reveals the important role played by pseudospin in determining the electronic structure.

The phenomenon of Rabi oscillations is well known in the context of two-level atomic systems in quantum optics [12–14] and also in conventional semiconductors [15]. We may expect graphene also to exhibit similar phenomena analogous to conventional semiconductors and two-level atomic systems. The nonlinear optics of graphene is a growing subject in condensed matter physics and material science. In fact, Ishikawa [16] has studied the nonlinear optical response of electron dynamics in single-layer graphene (SLG) in the time domain under the influence of intense light pulse and reported that the nonlinear optical response is not adequately described either by a pure intraband or by pure interband electron dynamics but, by their intermediate role. Using single-particle density matrix, Avetissian *et al* [17] presented a theoretical study of coherent nonlinear optical response of graphene under multiphoton interband excitation by pulsed laser field. The nonlinear optics of graphene is also described in the extensive literature available on this subject [18–25]. Ang *et al* [26] studied the nonlinear optics of BLG in the frequency range from the terahertz regime to the far-infrared regime and concluded that BLG is useful for developing graphene-based nonlinear photonics and optoelectronic devices. The optical properties of BLG are also described in [27,28]. A substantial amount of work has been done theoretically and experimentally on multilayer graphene (MLG) as well, which is described in various works [29–34].

The present work describes the nonlinear optics of BLG and MLG, specifically the phenomenon of ARO first predicted theoretically in SLG. Conventional Rabi oscillations in SLG have already been discussed in [16,17,21,22], using the rotating wave approximation (RWA). To analyse the phenomenon of ARO in BLG and MLG, an approximation called asymptotic rotating wave approximation (ARWA) has been invoked (which is an alternative to the rotating wave approximation). This alternative approach is able to reveal that for graphene-based systems, which possess pseudospin degrees of freedom, a second, anomalous, Rabi frequency is present. A comparison with an exactly solvable model identical to graphene in all respects except lacking in pseudospin shows that the anomalous Rabi frequency is peculiar to models with pseudospin [11]. The Bloch equations of graphene bilayer that confirm the presence of anomalous Rabi frequency are also solved numerically.

We now describe our theory of ARO in BLG and MLG.

2. Rabi oscillations in BLG

2.1 *Hamiltonian of BLG*

The effective low-energy two-component Hamiltonian of BLG describes the hopping between non-dimer sites A1–B2 (blue solid arrow) through dimer sites B1–A2 (green dashed arrow) (see figure 1a). The hopping between non-dimer sites A1–B2 includes the interlayer hopping (γ_1) and intralayer hopping (v). This effective low-energy Hamiltonian has been derived by McCann *et al* [4] using Green's function method for matrices.

$$\hat{H}_2 = -\frac{1}{2m}\begin{pmatrix} 0 & k_-^2 \\ k_+^2 & 0 \end{pmatrix}, \tag{1}$$

with the energy eigenvalues $E(\pm k) = \pm|k|^2/2m$, $\pm$ corresponds to the conduction and valance bands, respectively (see figure 1b). The eigenfunction of Hamiltonian eq. (1) in

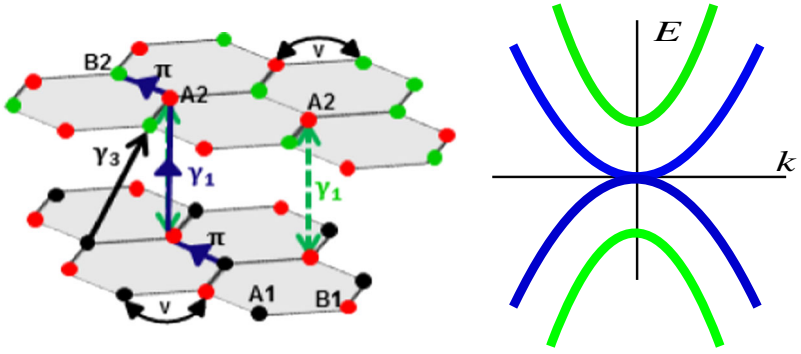

(a) (b)

Figure 1. (**a**) Honeycomb lattice structure of BLG containing four atoms per unit cell: A1 (black circles) and B1 (red circles) in the bottom layer and A2 (red circles) and B2 (green circles) in the top layer, respectively. (**b**) Schematic of the energy spectrum of BLG near K valley.

K valley can be represented as $\psi^T = (\psi_{A1}\psi_{B2})$, $k_\pm = k_x \pm i k_y$ and m is the effective mass of massive chiral Dirac fermions, $m = (\gamma_1/2v^2) \sim 0.035 m_e$. A semiclassical approach is used, radiation is treated classically and matter fields are quantum, to describe the phenomenon of ARO. An in-plane electric field is applied through a vector potential of the form $A_c(t) = A_c(0)\mathrm{e}^{-i\omega t}$, where $A_c(0) = (e/c)\left(A_x(0) + i\,A_y(0)\right)$ is the complex amplitude of the external applied field. This vector potential couples to BLG in a transverse gauge, and changes the momentum of massive Dirac fermions from $\mathbf{k}$ to $\mathbf{k} - (e/c)\mathbf{A}$. In second quantization, using two-component basis eigenstates of the Hamiltonian eq. (1) in momentum space of the form $\psi^T = (c_{A1}(\mathbf{k}, t)c_{B2}(\mathbf{k}, t))$, the Hamiltonian eq. (1) reads as

$$H = -\frac{1}{2m}\sum_{\mathbf{k}}\left[\left(k_- - A_c^*(t)\right)^2 c_{A1}^\dagger(\mathbf{k}, t)\, c_{B2}(\mathbf{k}, t) + \text{h.c.}\right], \tag{2}$$

where c and $c^\dagger$ are annihilation and creation operators on sublattice sites A1 and B2 in the bottom layer and top layer, respectively and vice versa.

2.2 *Derivation of Bloch equations*

In this section, we derive the Bloch equations which are the rate equations of polarization and population excess on sublattice sites A1 and B2. The fundamental dynamical quantities are: (i) the population difference $n_{\text{diff}}(\mathbf{k}, t)$ in the number densities of the A1 sublattice site in the bottom layer and the B2 sublattice site in the top layer and (ii) the interlayer polarization $p(\mathbf{k}, t)$. In terms of creation and annihilation operators, these quantities may be represented as

$$n_{\text{diff}}(\mathbf{k}, t) = \langle c_{A1}^\dagger(\mathbf{k}, t)c_{A1}(\mathbf{k}, t)\rangle - \langle c_{B2}^\dagger(\mathbf{k}, t)c_{B2}(\mathbf{k}, t)\rangle,$$

$$p(\mathbf{k}, t) = \langle c_{A1}^\dagger(\mathbf{k}, t)c_{B2}(\mathbf{k}, t)\rangle.$$

With the help of the equations of motion for operators, $i\,\partial_t\hat{\rho} = [\hat{\rho}, H]$, and simple anticommutator algebra for fermions, the Bloch equations of $n_{\text{diff}}(\mathbf{k}, t)$ and $p(\mathbf{k}, t)$ read as (setting $\hbar = 1$),

$$i\,\partial_t n_{\text{diff}}(\mathbf{k}, t) = -\frac{1}{m}\left[\left(k_- - A_c^*(0)\mathrm{e}^{i\omega t}\right)^2 p(\mathbf{k}, t) - \text{h.c.}\right], \tag{3}$$

$$i\,\partial_t p(\mathbf{k}, t) = -\frac{1}{2m}\left(k_+ - A_c(0)\mathrm{e}^{-i\omega t}\right)^2 n_{\text{diff}}(\mathbf{k}, t), \tag{4}$$

where $k_\pm = k_x \pm i k_y$ and $A_c(0) = (e/c)\left(A_x(0) + i\,A_y(0)\right)$. Equations (3) and (4) are also called the coherent optical Bloch equations for BLG. So the model presented here, is a pure coherent process of uncorrelated fermions.

2.3 *Solution of Bloch equations*

In this section, we discuss the solution of Bloch equations in the regions of interest. First, we solve these equations in off-resonance condition, when the external driving frequency

(EDF) ω is much larger than the interband transition frequency $2(|k|^2/2m)$ of the system ($\omega \gg |k|^2/m$). This situation is quite different from the conventional case, where the EDF is close to the particle–hole creation frequency. The conventional resonant case is already discussed in [16,22] on SLG. Here, we shall give only a qualitative description of this regime for the case of BLG.

Case I. Near the Dirac point (off-resonance: $\omega \gg \omega_{\mathrm{R}}$, $(2|k|^2/2m)$).

Here the Bloch equations are solved in the off-resonance regime using ARWA described in our earlier work. For that, we have to decompose $n_{\mathrm{diff}}(\mathbf{k}, t)$ and $p(\mathbf{k}, t)$ (e.g. see Boyd [13]) using the ansatz

$$n_{\mathrm{diff}}(\mathbf{k}, t) = n_s(\mathbf{k}, t) + \sum_{l=1}^{2} n_{fl}(\mathbf{k}, t)\mathrm{e}^{-il\omega t} + \text{c.c. of the 2nd term}, \tag{5}$$

$$p(\mathbf{k}, t) = p_s(\mathbf{k}, t) + \sum_{l=1}^{2} p_{l+}(\mathbf{k}, t)\mathrm{e}^{-il\omega t} + \text{c.c. of the 2nd term}. \tag{6}$$

Here, we retain terms varying as $\mathrm{e}^{\pm i\omega t}$ and $\mathrm{e}^{\pm 2i\omega t}$, unlike single-layer graphene, where we retain only the first harmonic, the underlying reason being that the ARO is associated with the second harmonic in BLG (at least for the population), while in SLG it is associated with the first harmonic. In BLG, the single harmonic may affect the second harmonic as multiplication of two single harmonics may give rise to the second harmonic. Hence, it is necessary to keep both the harmonics in external frequency, when decomposing $n_{\mathrm{diff}}(\mathbf{k}, t)$ and $p(\mathbf{k}, t)$ into slow and fast terms. Moreover, if we consider the Bloch equations for the case where $\mathbf{k} = 0$, it is clear that we have to keep terms at least up to second harmonic in external frequency, when decomposing the population and polarization into slow and fast terms.

We now insert this ansatz into the Bloch equations making a comparison of the same power in external frequency on both sides. In the analysis, we neglect terms containing harmonics larger than those present in the Hamiltonian of the system. Lastly, we assume that the EDF ω is very large compared to all other frequencies (so we can neglect the term $|\partial f/\partial t|$ in comparison to $\omega|f|$). These simplifications give the solution of the fast coefficients of population $n_{fl}(\mathbf{k}, t)$ and polarization $p_{l+}(\mathbf{k}, t)$ equations in terms of slow coefficients $n_s(\mathbf{k}, t)$ and $p_s(\mathbf{k}, t)$.

The slow varying part of the population and polarization equations comes out to be

$$i\,\partial_t n_s(\mathbf{k}, t) = -\frac{1}{m}\left[k_-^2 p_s(\mathbf{k}, t) - k_+^2 p_s^*(\mathbf{k}, t)\right],$$

$$i\,\partial_t p_s(\mathbf{k}, t) = -\frac{1}{2m}\left[k_+^2 n_s(\mathbf{k}, t) + \alpha p_s(\mathbf{k}, t)\right],$$

where $\omega_{\mathrm{R}} = |A_c(0)|^2/2m$. These equations may be solved by assuming that $n_s(\mathbf{k}, t) = n_s(\mathbf{k}, 0)\cos(2\Omega t)$ and $n_s(\mathbf{k}, 0) = 2|k_-|^2/\alpha$ is the equilibrium value of population, which

can be determined in mean-field approximation. This gives the solution for the slow part of polarization,

$$p_s(\mathbf{k},t) = \frac{k_+}{2k_-}\left[\cos(2\Omega t) + i\frac{4m\Omega}{\alpha}\sin(2\Omega t)\right],$$

$$\Omega = \left[\left(\frac{|k|^2}{2m}\right)^2 + \frac{\left(\omega_{\mathrm{R}}^2 + 4\frac{|k|^2\omega_{\mathrm{R}}}{m}\right)^2}{4\omega^2}\right]^{1/2}, \quad \alpha = \left(\frac{2m\omega_{\mathrm{R}}^2}{\omega} + \frac{8|k|^2\omega_{\mathrm{R}}}{\omega}\right).$$

$\Omega_{\mathrm{ARWA}}^{\mathrm{BLG}}(=2\Omega)$ is the generalized anomalous Rabi frequency for BLG in off-resonance. Exactly at Dirac point, $\mathbf{K} = 0$, the anomalous Rabi frequency comes out to be equal to, $\Omega_{\mathrm{ARF}} = \omega_{\mathrm{R}}^2/\omega$, where $\omega_{\mathrm{R}} = |A_c(0)|^2/2m$. This anomalous behaviour of Rabi frequency in off-resonance is attributed to pseudospin degree of freedom of BLG.

We may equally easily write the solution of Bloch eqs (3) and (4) in terms of slow coefficients $p_s(\mathbf{k},t)$ and $n_s(\mathbf{k},t)$ with the help of eqs (5) and (6) together with the fast coefficients.

Case II. Near-Dirac point (resonance case: $\nu\omega \approx 2(|k|^2/2m)$).

This subsection describes the solution of Bloch equations in the resonance regime when $\nu\omega$ is nearly equal to interband transition frequency. Here, there are two possible resonances – one is at the first harmonic in EDF, i.e. when $\nu = 1$ and the second resonance occurs due to the frequency doubling effect, i.e. when $\nu = 2$. To solve the Bloch equations in the resonance case, we applied a rotating wave approximation [13,15] well known in the context of two-level atomic systems in quantum optics. Mischenko [22] has also studied the phenomenon of Rabi oscillations for SLG in the case of small detuning, Δ, which is the difference between EDF and interband transition frequency of the system. His study shows a saturation behaviour of current density. In the case of small detuning, for BLG, the conventional Rabi frequency at the single harmonic (in which case, $\Delta \ll (\omega - 2(|k|^2/2m))$) and due to the frequency doubling effect (in which case, $\Delta \ll (2\omega - 2(|k|^2/2m))$), is given by, respectively,

$$\Omega_\omega = \left[\Delta^2 + 2\frac{|k|^2\omega_{\mathrm{R}}}{m}\right]^{1/2}, \ \Omega_{2\omega} = \left[\Delta^2 + \omega_{\mathrm{R}}^2\right]^{1/2},$$

$\Delta = \left(\nu\omega - 2(|k|^2/2m)\right)$, where $\nu = 1, 2$, respectively, for the first and second harmonic resonance (figure 2). In passing, we note that we have used complex exponential time-varying vector potentials, as opposed to real sinusoidal ones used by Mishchenko [22]. These two approaches are equivalent, when we consider linear equations but, for nonlinear systems such as the one we consider here, they are different. While Mischenko's approach has the appeal that it uses a physical real electric field, our approach has the appeal that the model with complex vector potentials (the Hamiltonians are real of course) is able to map the graphene system at resonance to the two-level system with the Rabi frequency given by the textbook value which depends on the electric field alone (it does not vanish in some

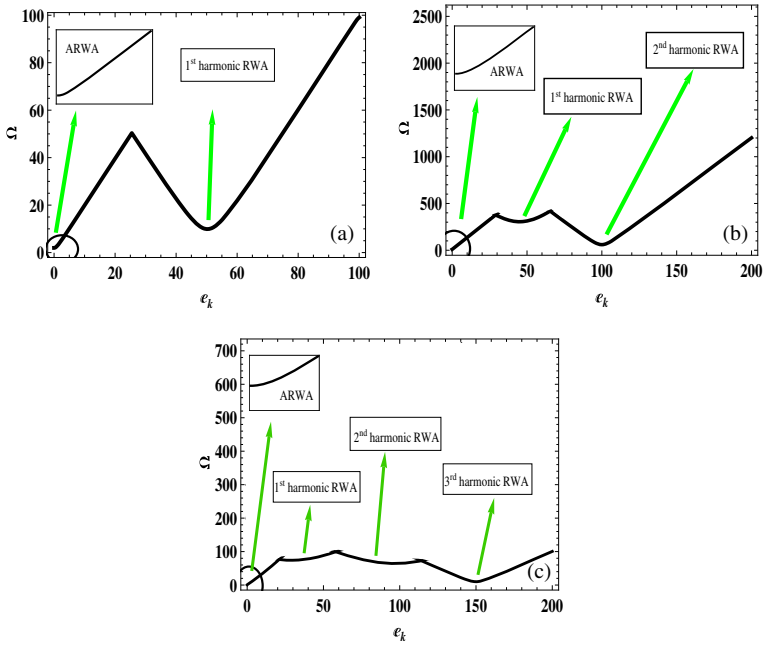

Figure 2. (**a**) Schematic of the effective Rabi frequency, Ω vs. band energy, $e_k = v_F|k|$ for single-layer graphene. In all the three plots, there is one anomalous Rabi frequency (ARF) close to $e_k = 0$. For a single layer, there is one conventional Rabi frequency (CRF) at $\omega = 2e_k$. (**b**) Schematic of the effective Rabi frequency, Ω vs. band energy, $e_k = |k|^2/2m$ for BLG. In addition to one ARF, two resonances (CRFs) are possible, one is at single harmonic ($\omega = 2e_k$) and the other is at second harmonic ($2\omega = 2e_k$) in external driving frequency. (**c**) Schematic of the effective Rabi frequency, Ω vs. band energy, $e_k = v_0^3|k|^3/\gamma_1^2$ for trilayer graphene. In addition to one ARF, three resonances are possible at values of e_k determined by $\nu\omega = 2e_k$, $\nu = 1, 2, 3$. The ARF plot near $e_k = 0$ gets flatter as the number of layers increases. Vertical axes (ordinates) are exaggerated for clarity. The analytical formulae behind these plots are given in Appendix B.

situations unlike Mishchenko's). Furthermore, our approach of using time-varying complex exponentials renders calculations involving higher harmonics (which is the norm in BLG and MLG) quite easy and elegant unlike what would be the case had we insisted on using real fields.

2.4 *Current density in BLG*

In this section, we discuss how to calculate the current density in ARWA regime. It is the current that is gauge-invariant and experimentally accessible. Using continuity equation $\nabla \cdot \mathbf{J}(\mathbf{r}, t) = -\partial_t \rho(\mathbf{r}, t)$, quantum kinetic equation $i\hbar\partial_t \rho(\mathbf{r}, t) = [\rho(\mathbf{r}, t), H]$ and Fourier

transform it, we may write the formula of current density for BLG in momentum space as (the average current is independent of position),

$$\langle \mathbf{J}(t)\rangle = \frac{1}{2\pi m}\sum_k \left[-\left((k_- - A_c^*(t))\,p(\mathbf{k},t) + \text{h.c.}\right)\right]\hat{x}$$
$$+i\frac{1}{2\pi m}\sum_k \left[\left((k_- - A_c^*(t))\,p(\mathbf{k},t) - \text{h.c.}\right)\hat{y}\right].$$

Inserting the value of $p(\mathbf{k},t)$, writing $k_\pm = |k|e^{\pm i\theta_k}$ and performing integration over θ_k, all the terms drop out except the terms which oscillate with the first harmonic in external applied field. Therefore, in the low-energy approximation, we may write the current density in frequency domain to exhibit a threshold behaviour.

$$j_x^s(\omega')|_{\text{ARWA}} \approx -\frac{A}{16\pi^2}\frac{\omega^2 A_c(0)}{32\omega_{\text{R}}^3}\left(\omega' - \frac{\omega_{\text{R}}^2}{\omega}\right)\theta\left(\omega' - \frac{\omega_{\text{R}}^2}{\omega}\right).$$

Near the threshold, when $\omega' \approx \omega_{\text{R}}^2/\omega$, the current density exhibits a linear behaviour (figure 3a). The exponent at the threshold of induced current in BLG is thus found to be equal to unity, whereas in SLG, this exponent has been computed [11] to be equal to $1/2$. The current density in both resonance cases is found to be

$$j_x^s(\omega')|_{\text{RWA},\omega} \approx \frac{A}{64\pi^2}\frac{A_c(0)}{\pi}\frac{\omega}{\sqrt{\omega'^2 - 2\omega\omega_{\text{R}}}},$$
$$j_x^s(\omega')|_{\text{RWA},2\omega} \approx \frac{A}{16\pi^2 m}\frac{A_c^4(0)}{8A_c^*(0)}\frac{1}{\sqrt{\omega'^2 - \omega_{\text{R}}^2}}.$$

The asymptotic forms of the current density in time domain in ARWA and RWA can be written as (figure 3b)

$$j_x^s(t)|_{\text{ARWA}} \approx \beta\frac{e^{-i(\omega_{\text{R}}^2/\omega)t}}{t^2}, \tag{7}$$

$$j_x^s(t)|_{\text{RWA},\omega} \approx \gamma\frac{\cos(\sqrt{2\omega\omega_{\text{R}}}\,t) - \sin(\sqrt{2\omega\omega_{\text{R}}}\,t)}{\sqrt{t}}, \tag{8}$$

$$j_x^s(t)|_{\text{RWA},2\omega} \approx \lambda\frac{\cos(\omega_{\text{R}}t) - \sin(\omega_{\text{R}}t)}{\sqrt{t}}, \tag{9}$$

where β, γ and λ are constants that fit the dimension of current density. So, it is obvious from eq. (7) that the slow part of the current density in off-resonance oscillates with the threshold frequency $\omega_{\text{R}}^2/\omega$ where the amplitude exhibits a power-law decay t^{-2}, whereas eqs (8) and (9) reveal that the slow part of the current density in RWA shows two different types of threshold behaviour, one is at the first harmonic and the other at the second harmonic in the external frequency. The corresponding Rabi frequencies are $(2\omega\omega_{\text{R}})^{1/2}$ and ω_{R}, respectively. The current density in both RWA cases has an amplitude that has a power-law decay of the form $t^{-1/2}$.

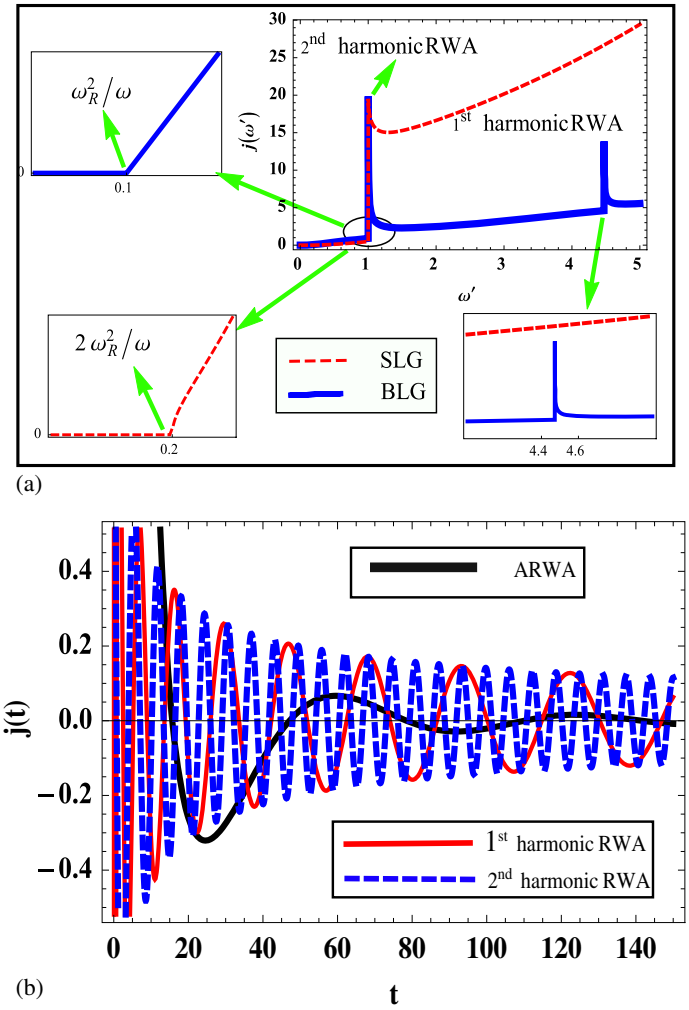

Figure 3. (**a**) Schematic of the variation of the slow part of the current density $j(\omega')$ with frequency ω' of BLG (blue solid curve) for zero-detuned Rabi frequency, $\omega_{\mathrm{R}} = 1$ in arbitrary units. The slow part of the current density exhibits threshold behaviour at the anomalous Rabi frequency, $\omega_{\mathrm{R}}^2/\omega$. Near threshold, the current density exhibits linear behaviour unlike SLG [11] (red dashed curve), where the current is proportional to the square root of the deviation from the resonant frequency (red dashed curve shown in the inset of the diagram). (**b**) This plot shows the variation of current density $j(t)$ with t. The solid black curve shows ARO in the time domain. The solid red and dashed blue lines show the first and second harmonic RWA case, respectively. The frequency associated with solid red and dashed blue curves are $\sqrt{2\omega\omega_{\mathrm{R}}}$ and ω_{R}, respectively.

3. Numerical simulation of the problem

In this section, we present a fully numerical simulation of the Bloch equations. Numerical simulation affirms the findings of the other sections discussed so far. We have employed

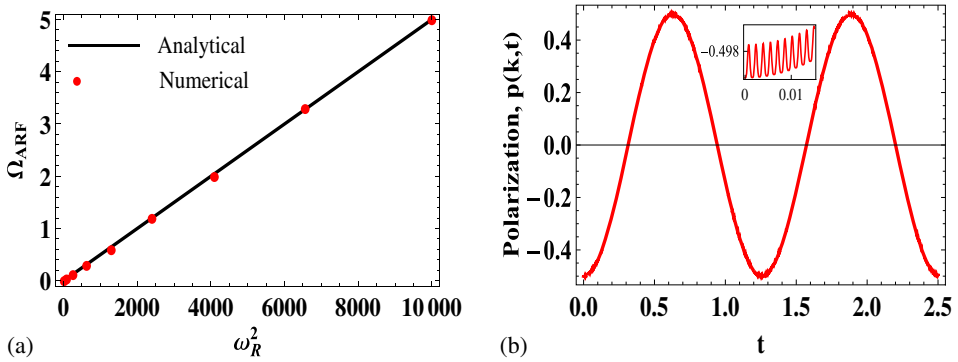

Figure 4. (**a**) Schematic of the variation of the anomalous Rabi frequency vs. $\omega_R^2 (= |A_c(0)|^4/4m^2) \sim$ square of the intensity of the applied field. The ARF found analytically (solid black line) is in good agreement with the numerical simulation (red dots). (**b**) It shows the slow as well as rapidly (inset) varying part of polarization $p(\mathbf{k}, t)$ vs. time t. For plotting purposes, we have chosen the parameters $(k_-/\sqrt{2m}) = 0$, $(A_c(0)/\sqrt{2m}) = 10$ and $\omega = 2000$, in arbitrary units. The frequency obtained from plot (**b**) is in complete agreement with analytical expectations.

the NDSolve routine of *Mathematica* to generate the plots of population and polarization with respect to time. The analytical (black line) anomalous Rabi frequency is in excellent agreement with the numerical simulation (red dots) (figure 4a). Far from resonance, the slow part of polarization oscillates exactly with the ARF that matches with the frequency inferred from numerical simulations (figure 4b). Figure 5 shows the numerical solution of Bloch equations in first harmonic resonance for population and polarization, respectively. The frequency of oscillation determined from the plot is consistent with the analytical result.

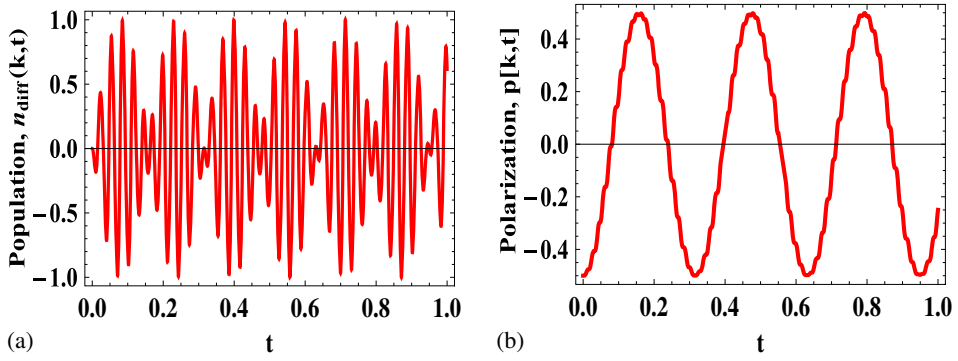

Figure 5. (**a**) and (**b**) Schematic of the slow- as well as rapidly-varying population, $n_{\text{diff}}(\mathbf{k}, t)$ and polarization $p(\mathbf{k}, t)$, respectively vs. time t at first harmonic resonance. The frequency of oscillation matches with the expectations from analytical solution. To plot, we have chosen the parameters, $(k_-/\sqrt{2m}) = 10$, $(A_c(0)/\sqrt{2m}) = 1$ and $\omega = 200$.

4. Rabi oscillations in twisted BLG

The earlier sections dealt with the phenomenon of Rabi oscillations in intrinsic BLG. This section describes the same phenomenon, when relative twisting between layers in BLG has been taken into account. Twisting, also called stacking defect, is unique to graphene with two or more layers. Twisted BLG shows drastically different electronic properties from that of AB-stacked BLG, as we have already mentioned in §1. We show that the ARF strongly depends on twist angle, and this dependence is most prominent for weak applied fields.

4.1 *Hamiltonian of twisted BLG*

The effective low-energy Hamiltonian of twisted BLG can be described by the two-column matrix as given below [7,35,36].

$$H^{\text{eff}}_{2,\text{twist}} = -\frac{2v_{\text{F}}^2}{15\tilde{t}_\perp}\begin{pmatrix} 0 & k_-^2 - (\Delta K_-/2)^2 \\ k_+^2 - (\Delta K_+/2)^2 & 0 \end{pmatrix}, \tag{10}$$

where $k_\pm = k_x \pm ik_y$, $\Delta K_\pm = \Delta K_x \pm i\Delta K_y$, v_{F} and $\tilde{t}_\perp$ are the Fermi velocities of the carriers and interlayer coupling, respectively. ΔK_x and ΔK_y define the relative shift between the corresponding Dirac points of the twisted BLG. Unlike in untwisted BLG, the band minimum in twisted BLG splits up into two and shows a linear band spectrum in the vicinity of these points (figure 6). Expanding Hamiltonian eq. (10) near $(\Delta K_\pm/2)$ by defining $k_\pm = q_\pm + (\Delta K_\pm/2)$, keeping terms up to quadratic in q, Hamiltonian eq. (10) reduces to the following form:

$$H^{\text{eff}}_{2,\text{twist}} = -\frac{2v_{\text{F}}^2}{15\tilde{t}_\perp}\begin{pmatrix} 0 & q_-^2 + q_-\Delta K_- \\ q_+^2 + q_+\Delta K_+ & 0 \end{pmatrix}. \tag{11}$$

Using Hamiltonian eq. (11) and following the same process as described in Case (I) of §2.3, we can find anomalous Rabi frequency in off-resonance case as given below:

$$\Omega_{\text{ARWA}} = 2\sqrt{E_k^2 + \frac{\left(\frac{|\alpha A_c^2(0)|^2}{\omega} + \frac{2\alpha^2}{\omega}|(2q_+A_c(0) + A_c(0)\Delta K_+)|^2\right)^2}{4}}, \tag{12}$$

where $E_k(\pm) = \pm|q_-^2 + q_-\Delta K_-|$ is the energy eigenvalue of the twisted BLG and $\alpha = 2v_{\text{F}}^2/15\tilde{t}_\perp$. Equation (12) gives the anomalous Rabi frequency near the shifted Dirac points in twisted BLG. If twist $\Delta K = 0$, we can get back the anomalous Rabi frequency of bilayer graphene without twist. Exactly at the shifted Dirac point, eq. (12) reduces to

$$\Omega_{\text{ARF}} = \left[\frac{\omega_{\text{R}}^2}{\omega} + \frac{2\omega_{\text{R}}}{\omega}\alpha|\Delta K|^2\right].$$

The variation of anomalous Rabi frequency at the shifted Dirac point with an external applied field and with the twist angle is clearly shown in the density plot in figure 7. It is seen that the anomalous Rabi frequency depends sensitively on the twist for weak applied fields (small ω_{R}).

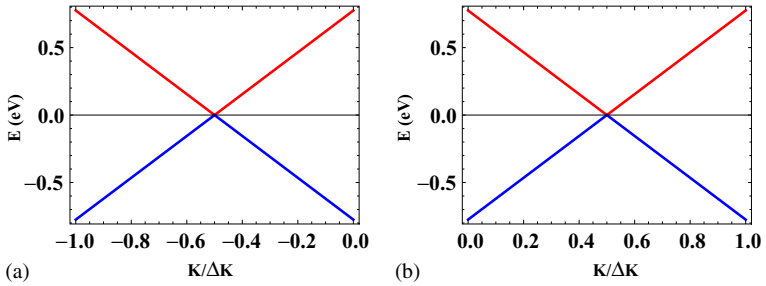

Figure 6. Schematic diagrams of band structure of twisted BLG: (**a**) for $q = K + \Delta K/2$ and (**b**) $q = K - \Delta K/2$. In the presence of twist, the Dirac point splits up into two Dirac points and shift by $\pm\Delta K/2$. For plotting purposes, we have taken the parameters: $v_F|\Delta K| = 1.56$ eV, twist angle $\theta = 10^\circ$ and $t_\perp = 0.22$ eV.

We have also solved the Bloch equations of twisted BLG in the resonant case. A similar process is adopted to solve the Bloch equations as described in Case (II) of §2.3. The conventional Rabi frequencies near the first and second harmonic resonances are found to be, respectively,

$$\Omega_\omega = \sqrt{\Delta^2 + \omega_R\left(\alpha|q_+|^2 + \alpha|\Delta K_-|^2 + \alpha q_+ \Delta K_- + \alpha q_- \Delta K_+\right)},$$

$$\Omega_{2\omega} = \sqrt{\Delta^2 + \omega_R^2},$$

$$\Delta = \omega - 2E_k, \quad E_k = |\alpha q_-^2 + \alpha q_- \Delta K_-|, \quad \omega_R = \alpha|A_c(0)|^2, \quad \alpha = \frac{2v_F^2}{15\tilde{t}_\perp}.$$

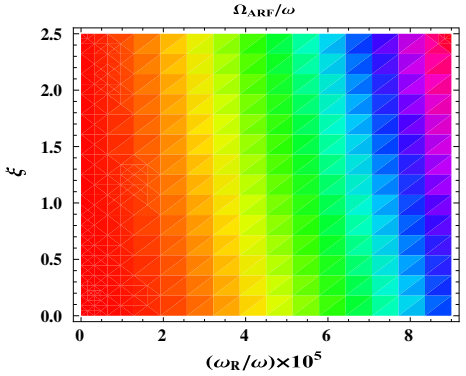

Figure 7. This density plot shows dimensionless anomalous Rabi frequency Ω_{ARF}/ω vs. ω_R/ω and $\xi(= \hbar\alpha|\Delta K|^2/\omega)$ at the shifted Dirac point. It is clear from the figure that twisting is prominent for weak applied fields. The value of $\hbar\Omega_{ARF}$ for red, green and blue colours are 3.7×10^{-5}, 1.84×10^{-4} and 2.97×10^{-4} eV, respectively, at a fixed value of $\xi = 1.5$.

Table 1. Realistic values of various energy scales in monolayer, bilayer and twisted BLG are shown. The numerical values of all parameters are determined at a fixed value of external frequency, $\omega = 6\pi \times 10^{14}$ rad/s and an applied electric field, $|E| = 250$ kV/cm.

Energy	Unit (eV)		
	SLG	BLG	TBLG
$\hbar\omega_{\mathrm{R}}^2/\omega$	1.4×10^{-4}	1.78×10^{-7}	8.8×10^{-8}
$\hbar\omega_{\mathrm{R}}$	1.3×10^{-2}	4.69×10^{-4}	1.05×10^{-4}
$\hbar\Omega_{\mathrm{ARF}}$	2.8×10^{-4}	1.78×10^{-7}	5.02×10^{-5}
$\hbar(\hbar\alpha\|\Delta K\|^2)$	–	0	2.9
$\hbar\omega$	1.24	1.24	1.24

Similar to BLG, twisted BLG also shows harmonic resonances. Twist has effect only on first harmonic resonance while second harmonic resonance is not affected by twisting as we can see from eq. (11). We just saw that the anomalous Rabi frequency is greatly affected by the twist, whereas conventional Rabi frequency is less affected. This is because at resonance q is not small, rather it is given by the condition $2|\alpha q_-^2 + \alpha q_- \Delta K_-| = \omega$. Thus, we see that while the anomalous Rabi frequency with twist is $\propto \omega_{\mathrm{R}}$ for small fields and $\propto \omega_{\mathrm{R}}^2$ without twist, the conventional Rabi frequency continues to have the form $\propto \sqrt{(\cdot\cdot) + \omega_{\mathrm{R}}(\cdot\cdot)}$, both with and without twist.

Lastly, we examine the effect of a small voltage between layers. The low-energy electronic spectrum of twisted BLG in the presence of a small bias (voltage) ($V \ll v_{\mathrm{F}}|\Delta K|$) between the layers has already been discussed by Lopes *et al* [7]. They found that the system continues to be gapless and the dispersion is linear with the same Fermi velocity as twisted bilayer without bias, but the Dirac points shift vertically by $\sim \pm V/3$. Thus, our predictions for the anomalous Rabi frequency in this case are unchanged. A comparison of the various parameters in single-layer, bilayer and twisted bilayer graphene is given in table 1.

So far, we have ignored long-range Coulomb interactions. A natural question that one can pose next is – how would these predictions be affected by the inclusion of long-range Coulomb interactions? This is especially important in doped systems where a finite density of carriers is present, bearing in mind also that in graphene, screening is weak. The theoretical analysis and interpretation of experimental data are complicated in such a situation. To avoid this, we work with undoped systems and probe the phenomena of anomalous Rabi oscillations using pump–probe experiments. Here, a small density of carriers are created transiently, which means that the dominant effect is the same as what has been discussed in the earlier supporting papers. Therefore, even though the phenomenon of ARO may be modified by including many-body effects, it will still remain a defining characteristic of systems possessing pseudospin. A detailed theoretical analysis of the pump–probe experiment is given in [37].

5. Multilayer graphene

Here, we describe how to generalize the ideas of the previous discussion to n-layer graphene, also known as multilayer graphene (MLG) [29]. MLG can be formed by the

stacking of single graphene sheets one above the other – either in ABAB... arrangement (Bernal stacking) or ABCABC... pattern (rhombohedral stacking) (see figure 8). For the present discussion, Bernal stacking is considered. These layers are weakly coupled by Van der Waals force. In terms of second quantization, the effective low-energy Hamiltonian for n-layer graphene [4,38,39] may be written as

$$H_n = \lambda \sum_{\mathbf{k}} \sum_{j=1}^{n-1} \left[K_-^n c_{\mathrm{A}j}^\dagger(\mathbf{k}, t) c_{\mathrm{B}(j+1)}(\mathbf{k}, t) + \text{h.c.} \right],$$

where $\lambda = v_0^n/(-\gamma_1)^{(n-1)}$, $K_- = k_- - A_c^*(0)\mathrm{e}^{i\omega t}$, $K_+ = K_-^*$, $k_\pm = k_x \pm ik_y$, $A_c(0) = (e/c)(A_x(0) + iA_y(0))$ is the complex vector potential which couples to MLG in the transverse gauge, $(\nabla \cdot \mathbf{A} = 0)$. The index n starts from $n = 2, 3, 4, ...$ for two, three, four layers, respectively. The single layer $n = 1$ is a special case, which we have already dealt with separately [11]. Nevertheless, we may recover the single-layer graphene Hamiltonian by setting $n = 1$ and removing the summation and all the indices. The symbol 'j' denotes the effective interlayer hopping between non-dimer states through the dimer states. This is accomplished by coupling the jth layer to the $(j + 1)$th layer.

5.1 *Bloch equations for n-layer graphene*

Following a procedure similar to the one described in §2.2, Bloch equations are easily derived for MLG. Just as in BLG, here too, we define dynamical quantities such as population and polarization as shown below.

$$N_{\nu\,\nu+1}(\mathbf{k}, t) = \langle c_{\mathrm{A}\nu}^\dagger(\mathbf{k}, t) c_{\mathrm{A}\nu}(\mathbf{k}, t)\rangle - \langle c_{\mathrm{B}(\nu+1)}^\dagger(\mathbf{k}, t) c_{\mathrm{B}(\nu+1)}(\mathbf{k}, t)\rangle,$$

$$\pi_{\nu\,\nu+1}(\mathbf{k}, t) = \langle c_{\mathrm{A}\nu}^\dagger(\mathbf{k}, t) c_{\mathrm{B}(\nu+1)}(\mathbf{k}, t)\rangle,$$

where the index $\nu = 1, 2, ...$ labels a layer in MLG. If $\nu = 1$, two graphene layers will be involved and if $\nu = 2$, three graphene layers will be involved and so on.

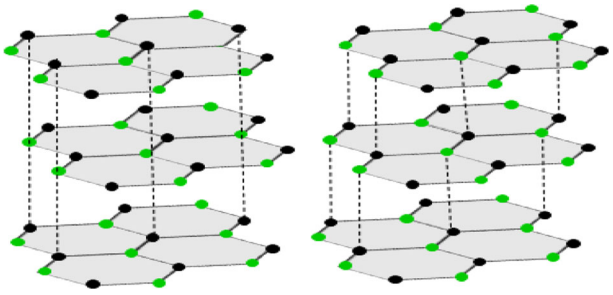

(a) (b)

Figure 8. Schematic diagrams of few-layer graphene crystal structure: (**a**) ABAB... arrangement (Bernal stacking) and (**b**) ABC.... arrangement (rhombohedral stacking). A and B correspond to green and black circles respectively.

The quantum kinetic equations for $N_{\nu\,\nu+1}(\mathbf{k}, t)$ and $\pi_{\nu\,\nu+1}(\mathbf{k}, t)$ of n-layer graphene read as

$$i\,\partial_t N_{\nu\,\nu+1}(\mathbf{k}, t) = \lambda\left[2K_-^n\,\pi_{\nu\,\nu+1}(\mathbf{k}, t) - \text{h.c.}\right],$$

$$i\,\partial_t \pi_{\nu\,\nu+1}(\mathbf{k}, t) = \lambda K_+^n N_{\nu\,\nu+1}(\mathbf{k}, t).$$

These are the coherent optical Bloch equations of multilayer graphene.

5.2 *Solution of Bloch equations*

In the present case of n-layer graphene, we follow the same procedure as earlier for bilayer and work out the solutions at the Dirac point (far from resonance), near the Dirac point and finally close to resonance.

Case I: At Dirac point, $\mathbf{k} = 0$.

At the Dirac point, $\mathbf{k} = 0$, the coupled Bloch equations for n-layer graphene may be solved using an ansatz, $\pi_{\nu\,\nu+1}(\mathbf{0}, t) = \pi_{\nu\,\nu+1,\,s}(\mathbf{0}, t)\mathrm{e}^{-in\omega t}$. Making this substitution and performing a straightforward calculation, we may write the solution of Bloch equations

$$N_{\nu\,\nu+1}(\mathbf{0}, t) = \frac{4\lambda(-A_c(0))^n}{n\omega}\pi^*_{\nu\,\nu+1,\,s}(\mathbf{0}, 0)\sin(\Omega_{\mathrm{R}}t),$$

$$\pi^*_{\nu\,\nu+1,\,s}(\mathbf{0}, t) = \pi^*_{\nu\,\nu+1,\,s}(\mathbf{0}, 0)\mathrm{e}^{-i\Omega_{\mathrm{R}}t},\ \Omega_{\mathrm{R}} \approx n\omega + \Omega^{\mathrm{NLG}}_{\mathrm{ARF}},$$

where $\Omega^{\mathrm{NLG}}_{\mathrm{ARF}} = 2\omega_{\mathrm{R}}^2/n\omega$ is the generalized ARF for n-layer graphene at the Dirac point with which the slow part of polarization oscillates and $\omega_{\mathrm{R}} = \lambda|A_c(0)|^n$. As we have been stressing, this ARF is observable only in systems that possess a pseudospin degree of freedom. One may see that while the ARO in polarization appears to be associated with the nth harmonic in the EDF ω for n-layer graphene, in reality, the overall polarization $p(\mathbf{0}, t)$ is slowly varying on the scale of the EDF. However, the population does oscillate according to the nth harmonic in EDF.

Case II: Near the Dirac point (off-resonance, $\omega \gg \omega_{\mathrm{R}}, \lambda|k|)^n$).

Following §2.3 Case (I), we discuss how to solve the Bloch equations for n-layer graphene using the ARWA method discussed earlier. The main assumption involved in ARWA is that the EDF ω is the largest frequency. In order to solve the Bloch equations, we decomposed population $N_{\nu\,\nu+1}(\mathbf{k}, t)$ and polarization $\pi_{\nu\,\nu+1}(\mathbf{k}, t)$ into slow- and fast-varying equations, as we did for BLG. But, this time the summation over l will run from $l = 1$ to $l = n$. In SLG, AROs are observed at the level of first harmonic, whereas in BLG these are observed at second harmonic. Therefore, it forces us to keep all the harmonics in the case of n-layer graphene to see the ARO. Inserting these equations in the Bloch equations and following a process of §2.3 for off-resonance, we may easily write down

the solution for the rapidly-varying polarization and population equations in terms of their slowly-varying coefficients. The slowly-varying part of population and polarization equation will be

$$i\,\partial_t N_s(\mathbf{k},t) \;=\; 2\lambda k_-^n \pi_s(\mathbf{k},t) - 2\lambda k_+^n\, \pi_s^*(\mathbf{k},t),$$

$$i\,\partial_t \pi_s(\mathbf{k},t) \;=\; \lambda k_+^n N_s(\mathbf{k},t) - 2\beta \pi_s(\mathbf{k},t).$$

With the help of these two equations and assuming that the solution for the slow part of population equation $N_s(\mathbf{k},t) = N_s(\mathbf{k},0)\cos(2\Omega t)$, we may write the solution for the slow part of polarization as

$$\pi_s(\mathbf{k},t) \;=\; \pi_s(\mathbf{k},0)\left[-i\frac{\beta}{\Omega}\cos(2\Omega t) + \sin(2\Omega t)\right],$$

$$\Omega = \left[\lambda^2|k|^{2n} + \beta^2\right]^{1/2}, \quad \beta = \sum_{l=1}^{n} \frac{(\lambda C_l^n)^2 |k|^{2(n-l)} |A_c(0)|^{2l}}{l\omega}, \tag{13}$$

where $\Omega_{\mathrm{ARWA}}^{\mathrm{NLG}}(=2\Omega)$ is the generalized anomalous Rabi frequency for n-layer graphene and $\pi_s(\mathbf{k},0) = (-1)^n(k_+^n/2|k|^n)$ and $N_s(\mathbf{k},0) = -((-1)^n\lambda|k|^n/\beta)$ are the equilibrium values of polarization and population, and may be determined in the mean-field approximations.

Case III: Near-resonance ($\omega \approx 2\lambda|k|)^n$).

This section deals with the solution of Bloch equations in the resonance case for small detuning, $\Delta \ll (\nu\omega - 2\lambda|k|^n)$, where ν denotes the number of resonances present in the particular graphene system, i.e. if $n = 1$ then $\nu = 1$ and only one resonance will be present, for BLG $n = 2$, two resonances will occur. The one at $\nu = 1$ occurs at single harmonic in EDF and the one at $\nu = 2$ is due to a frequency doubling effect in BLG which is absent in SLG and so on. First, we write the Bloch equations in matrix form, then find the diagonalization matrix of the time-independent part of the Hamiltonian, thereafter use the appropriate substitutions to solve the Bloch equations (see Appendix A). The conventional Rabi frequency comes out to be

$$\Omega_{\mathrm{RWA}}^{\mathrm{NLG}} = \sqrt{\Delta^2 + \omega_{\mathrm{R}}^2}, \quad \omega_{\mathrm{R}} = \lambda C_\nu^n |A_c(0)|^\nu |p|^{n-\nu}, \tag{14}$$

where $C_\nu^n = n!/\nu!(n-\nu)!$ are combinatorial factors.

5.3 *Current density in n-layer graphene*

In order to compute the current density for n-layer graphene, we adopt a procedure similar to the one discussed in §2.4 for the case of BLG. We can derive a formula of current density of the νth layer for MLG which will be of the form, $\langle J_\nu(t)\rangle = J_x\hat{x} + J_y\hat{y}$. Here J_x, J_y are defined as $J_{\nu,\pm} = J_x \pm i\,J_y$, where $J_{\nu,+}$ reads as

$$\langle J_{\nu,+}(t)\rangle = \frac{2n\lambda}{2\pi} \sum_{\mathbf{k}} \sum_{l=0}^{n-1} C_l^{n-1} k_-^{n-1-l} (-A_c^*(0))^l \mathrm{e}^{il\omega t} \pi_{\nu\,\nu+1}(\mathbf{k},t).$$

Inserting the value of $\pi_{v\,v+1}(\mathbf{k}, t)$ in the above equation gives

$$\langle J_{v,+}(t)\rangle = -\frac{n\lambda}{\pi}\sum_{\mathbf{k}}\frac{(-1)^n|k|^n}{(-A_c^*(0))}\cos(\Omega_{\mathrm{ARWA}}^{\mathrm{NLG}}t)\mathrm{e}^{-i\omega t}. \tag{15}$$

Equation (15) is our basic equation to find the current density in n-layer graphene. In the low-energy approximation, the current density in frequency domain will be

$$\langle J_{v,+}(\omega')\rangle = J_0\left(\omega' - \frac{2\omega_{\mathrm{R}}^2}{n\omega}\right)^{n/2}, \tag{16}$$

where J_0 is a constant that fits the dimension of current density. It must be stressed that the current density in eq. (16) is valid only in low-energy approximations and near the threshold, when $\omega' \approx 2\omega_{\mathrm{R}}^2/n\omega$. Moreover, eq. (16) is not valid for $n = 1$ (SLG) which is a special case already discussed in an earlier work. Nevertheless, we may calculate the current density directly by the general eq. (15), even for $n = 1$.

6. Conclusions

In conclusion, the phenomenon of anomalous Rabi oscillations (ARO) in bilayer (with and without twist) and multilayer graphene was discussed in the presence of an intense electromagnetic field. As expected, we found that the anomalous Rabi frequency is highly sensitive to the low-energy band structure and therefore, depends strongly on the twist, whereas the conventional Rabi frequency, applicable near resonance which occurs far from the bottom of the bands, is much less affected by the twist. Thus, anomalous Rabi oscillations are useful barometers for studying low-energy electronic structure of graphene-based systems. Unlike other methods such as ARPES which only confirm that the graphene dispersion is linear, ARO also reveals the important role played by pseudospin in determining the electronic structure. Only one anomalous Rabi frequency is associated with each graphene system, whereas multilayer graphene shows multiple conventional harmonic resonances depending on the system chosen. Furthermore, the anomalous Rabi frequency in these systems has a different dependence on the external electric field from the conventional one. ARO in all these systems are attributable to the pseudospin degree of freedom that they possess.

Appendix A

In this section, we present the solution of Bloch equations at resonance for multilayer graphene. The general Bloch equations for n-layer graphene are

$$\begin{aligned}
i\,\partial_t N(t) &= 2\lambda\left[(k_- - A_c^*(t))^n\pi(t) - (k_+ - A_c(t))^n\pi^*(t)\right],\\
i\,\partial_t\pi(t) &= \lambda\,(k_+ - A_c(t))^n\,N(t), \quad i\,\partial_t\pi^*(t) = -\lambda\big(k_- - A_c^*(t)\big)^n\,N(t),\\
A_c(t) &= \frac{e}{c}\left(A_x(0) + i\,A_y(0)\right)\mathrm{e}^{-i\omega t} = A_c(0)\mathrm{e}^{-i\omega t}, \qquad \lambda = \frac{v_0^n}{(-\gamma_1)^{n-1}}.
\end{aligned}$$

The above equations exhibit what may be termed as 'harmonic resonances'. Their description is as follows. First, we diagonalize a time-independent matrix formed by the Bloch equations, when the external field is absent, and that may be diagonalized by making the substitution,

$$\begin{pmatrix} N \\ \pi \\ \pi^* \end{pmatrix} = \begin{pmatrix} 0 & 2\frac{|k|^n}{k_-^n} & -2\frac{|k|^n}{k_-^n} \\ \frac{|k|^{2n}}{k_-^{2n}} & -\frac{|k|^{2n}}{k_-^{2n}} & -\frac{|k|^{2n}}{k_-^{2n}} \\ 1 & 1 & 1 \end{pmatrix} \begin{pmatrix} \tilde{N} \\ \tilde{\pi} \\ \tilde{\pi}^* \end{pmatrix}.$$

Now, the full Bloch equations may be written in a matrix form as follows:

$$i\,\partial_t \begin{pmatrix} N \\ \pi \\ \pi^* \end{pmatrix} = \begin{pmatrix} 0 & 2\lambda k_-^n & -2\lambda k_+^n \\ \lambda k_+^n & 0 & 0 \\ -\lambda k_-^n & 0 & 0 \end{pmatrix} \begin{pmatrix} N \\ \pi \\ \pi^* \end{pmatrix} + \sum_{m=1}^{n} C_m^n \begin{pmatrix} 0 & 2(b_1)_{12} & -2(b_1)_{12}^* \\ (b_1)_{12}^* & 0 & 0 \\ -(b_1)_{12} & 0 & 0 \end{pmatrix} \begin{pmatrix} N \\ \pi \\ \pi^* \end{pmatrix},$$

where

$$(b_1)_{12} = \lambda k_-^{n-m}(-A_c^*(t))^m \quad \text{and} \quad C_m^n = \frac{n!}{(n-m)!m!}$$

are combinatorial factors. Now, we transform to the new variables.

In this case, we retain only one value of m in the above equation, denoted by $m = \nu$, anticipating that the resonance will occur for that particular value of ν for which $\nu\omega = 2\lambda|k|^n$. The other values of ν are far from resonance for the value of $|k|$ obeying this equation. In such a situation we may write

$$i\,\partial_t \tilde{N}(t) = C_\nu^n(-)^\nu(-a\tilde{\pi}(t) + a\tilde{\pi}^*(t)),$$

$$i\,\partial_t \tilde{\pi}(t) = -2\lambda|k|^n\,\tilde{\pi}(t) + C_\nu^n(-)^\nu\left(\frac{1}{2}a\tilde{N}(t) - b\tilde{\pi}(t)\right),$$

$$i\,\partial_t \tilde{\pi}^*(t) = 2\lambda|k|^n\tilde{\pi}^*(t) + C_\nu^n(-)^\nu\left(-\frac{1}{2}a\tilde{N}(t) + b\tilde{\pi}^*(t)\right),$$

where

$$a \equiv |k|^n\lambda(-k_+^{-\nu}(A_c(t))^\nu + k_-^{-\nu}(A_c^*(t))^\nu),$$

$$b = |k|^n\lambda(k_+^{-\nu}(A_c(t))^\nu + k_-^{-\nu}(A_c^*(t))^\nu).$$

Rotating wave approximation involves using $\tilde{\pi}(\vec{k},t) = \mathrm{e}^{2it\lambda|k|^n}\,\tilde{\pi}'(\vec{k},t)$ and using $\nu\omega - 2\lambda|k|^n \equiv \Delta \ll \nu\omega$ so that

$$
\begin{aligned}
i\,\partial_t\tilde{\pi}'(t) &= C_\nu^n(-)^\nu\left(\frac{1}{2}|k|^n\lambda(k_-^{-\nu}(A_c^*)^\nu \mathrm{e}^{i\,\Delta t})\tilde{N}(t)\right),\\
i\,\partial_t\tilde{N}(t) &= C_\nu^n(-)^\nu|k|^n\lambda(k_+^{-\nu}(A_c)^\nu \mathrm{e}^{-i\,\Delta t}\;\tilde{\pi}'(t) + \text{h.c.}),\\
\tilde{\pi}'(\mathbf{k},t) &= \mathrm{e}^{i\,\Delta t}\Pi(\mathbf{k},t),\\
i\,\partial_t\Pi(t) - \Delta\Pi(t) &= C_\nu^n(-)^\nu\;\;\frac{1}{2}|k|^n\lambda k_-^{-\nu}(A_c^*)^\nu\tilde{N}(t),\\
i\,\partial_t\tilde{N}(t) &= C_\nu^n(-)^\nu(-|k|^n\lambda(-k_+^{-\nu}(A_c)^\nu)\Pi(t) + \text{h.c.}),\\
\Pi(\mathbf{k},t) &= \frac{\mathrm{e}^{i\pi\nu}|k|^n k_-^{-\nu}\lambda\tilde{N}(\mathbf{k},0)C_\nu^n\Delta(-1+\cos(\Omega t) - i\,\Omega\,\sin(\Omega t))(A_c^*)^\nu}{2\Omega^2},\\
\tilde{N}(\mathbf{k},t) &= \tilde{N}(\mathbf{k},0)\frac{\Delta^2 + (\Omega^2-\Delta^2)\cos(\Omega t)}{\Omega^2},\\
\Omega^{\mathrm{NLG}} &= \sqrt{\Delta^2+\omega_{\mathrm{R}}^2},\quad \omega_{\mathrm{R}} = \lambda C_\nu^n|A_c(0)|^\nu|k|^{(n-\nu)}.
\end{aligned}
$$

Appendix B

In this section, we describe the analytical expressions used for generating the central result of our work, viz. figure 2. All the three parts of figure 2 are obtained through a numerical solution of the nonlinear equation for the eigenfrequency (see our earlier work [11]). In our earlier work, we showed that the plots are equally well represented by a simple smooth interpolation of subplots applicable in different regimes, where analytical expressions are possible (the last four equations on p. 4606 of that work). Here too, we adopt the same strategy to obtain:

(a) For single-layer graphene:

$$
\begin{aligned}
\Omega_{\mathrm{SLG}}\left(v_{\mathrm{F}}|\mathrm{k}| < \frac{\omega}{4}\right) &= 2\sqrt{(v_{\mathrm{F}}|k|)^2 + \frac{\omega_{\mathrm{R}}^4}{\omega^2}},\\
\Omega_{\mathrm{SLG}}\left(\frac{\omega}{4} < v_{\mathrm{F}}|k|\right) &= \sqrt{(\omega - 2v_{\mathrm{F}}|k|)^2 + \omega_{\mathrm{R}}^2}.
\end{aligned}
$$

The conventional Rabi frequency is related to the fields in single-layer graphene through $\omega_{\mathrm{R}} = v_{\mathrm{F}}|\frac{e}{c}\vec{\sigma}_{\mathrm{BA}}\cdot\vec{A}(0)|$.

(b) For BLG:

$$
\begin{aligned}
\Omega_{\mathrm{BLG}}\left(\frac{|k|^2}{2m} < \frac{\omega}{4}\right) &= 2\sqrt{\left(\frac{|k|^2}{2m}\right)^2 + \frac{\left(\omega_{\mathrm{R}}^2 + 8\frac{|k|^2\omega_{\mathrm{R}}}{2m}\right)^2}{4\omega^2}},\\
\Omega_{\mathrm{BLG}}\left(\frac{\omega}{4} < \frac{|k|^2}{2m} < \frac{3\omega}{4}\right) &= \sqrt{\left(\omega - 2\frac{|k|^2}{2m}\right)^2 + 4\frac{|k|^2\omega_{\mathrm{R}}}{2m}},\\
\Omega_{\mathrm{BLG}}\left(\frac{3\omega}{4} < \frac{|k|^2}{2m}\right) &= \sqrt{\left(2\omega - 2\frac{|k|^2}{2m}\right)^2 + \omega_{\mathrm{R}}^2},\quad \omega_{\mathrm{R}} = \frac{|A_c(0)|^2}{2m}.
\end{aligned}
$$

(c) for trilayer graphene:

$$\Omega_{\mathrm{TLG}}\left(\alpha|k|^3 < \frac{\omega}{4}\right) = 2\frac{\sqrt{\left(\omega'_{\mathrm{R}}\right)^2 + \alpha^2|k^3|^2\omega^2}}{\omega},$$

$$\omega'_{\mathrm{R}} = \left(9\alpha^2|k|^4\left(\frac{\omega_{\mathrm{R}}}{\alpha}\right)^{2/3} + \frac{9}{2}\alpha^2|k|^2\left(\frac{\omega_{\mathrm{R}}}{\alpha}\right)^{4/3} + \frac{1}{3}\omega_{\mathrm{R}}^2\right),$$

$$\Omega_{\mathrm{TLG}}\left(\frac{\omega}{4} < \alpha|k|^3 < \frac{3\omega}{4}\right) = \sqrt{\Delta^2 + 9\omega_{\mathrm{R}}^{2/3}\left(\alpha|k|^3\right)^{4/3}},$$

$$\Omega_{\mathrm{TLG}}\left(\frac{3\omega}{4} < \alpha|k|^3 < \frac{5\omega}{4}\right) = \sqrt{\Delta^2 + 9\omega_{\mathrm{R}}^{4/3}\left(\alpha|k|^3\right)^{2/3}},$$

$$\Omega_{\mathrm{TLG}}\left(\frac{5\omega}{4} < \alpha|k|^3\right) = \sqrt{\Delta^2 + \omega_{\mathrm{R}}^2}, \qquad \omega_{\mathrm{R}} = \frac{v_0^3}{\gamma_1^2}|A_c(0)|^3,$$

where $\Delta = \left(\nu\omega - 2\alpha|k|^3\right)$. $\nu = 1, 2, 3$ for first, second and third harmonic resonances, respectively. These formulae clearly show the harmonic resonances associated with conventional Rabi oscillations.

References

[1] K S Novoselov, A K Geim, S V Morozov, D Jiang, Y Zhang, S V Dubonos, I V Grigorieva and A A Firsov, *Science* **306**, 666 (2004)
[2] P R Wallace, *Phys. Rev.* **71**, 622 (1947)
[3] A K Giem and K S Novoselov, *Nat. Mater.* **6**, 183 (2007)
[4] E McCann and V I Fal'ko, *Phys. Rev. Lett.* **96**, 086805 (2006)
[5] M Mucha-Kruczynski, E McCann and V I Fal'ko, *Semicond. Sci. Technol.* **25**, 033001 (2006)
[6] E McCann, D S L Aberger and V I Fal'ko, *Eup. Phys. J.: Special Topic* **148**, 91 (2006)
[7] J M B Lopes dos Santos, N M R Peres and A H Castro Neto, *Phys. Rev. Lett.* **99**, 256802 (2007)
[8] G Li, A Luican, J M B Lopes dos Santos, A H Castro Neto, A Reina, J Kong and E Andrei, *Nat. Phys.* **6**, 109 (2009)
[9] A Luican, G Li, A Reina, J Kong, R Nair, K S Novoselov, A K Geim and E Andrei, *Phys. Rev. Lett.* **106**, 126802 (2011)
[10] W Yan, M Lui, R F Dou, L Meng, L Feng, Z D Chu, Y F Zhang, Z F Lui, J C Nie and L He, *Phys. Rev. Lett.* **109**, 126801 (2012)
[11] Enamullah, V Kumar and G S Setlur, *Physica B* **407**, 4600 (2012)
[12] I I Rabi, *Phys. Rev.* **51**, 652 (1937)
[13] R W Boyd, *Nonlinear optics* (Singapore, Elsevier, 2009)
[14] L Allen and J H Eberly, *Optical resonances and two-level atoms* (Wiley and Sons, New York, 1975)
[15] H Haug and S W Koch, *Quantum theory of optical and electronic properties of semiconductors*, 4th edn (World Scientific, Singapore, 2004)
[16] K L Ishikawa, *Phys. Rev. B* **82**, 201402 (2010)
[17] H K Avetissian, A K Avetissian, G F Mkrtchian and Kh V Sedrakian, *Phys. Rev. B* **85**, 115443 (2012)
[18] X Yao and A Belyanin, *Phys. Rev. Lett.* **108**, 255503 (2012)
[19] B Dora, K Ziegler, P Thalmeier and M Nakamura, *Phys. Rev. Lett.* **102**, 036803 (2009)

[20] A R Wright, X G Xu, J C Cao and C Zhang, *Appl. Phys. Lett.* **95**, 072101 (2009)
[21] P N Romanets and F T Vasko, *Phys. Rev. B* **81**, 241411 (2010)
[22] E G Mishchenko, *Phys. Rev. Lett.* **103**, 246802 (2009)
[23] Y Zhou and M W Wu, *Phys. Rev. B* **83**, 245436 (2011)
[24] S A Mikhailov, *Physica E* **40**, 2626 (2008)
[25] S A Mikhailov, *Physica E* **44**, 924 (2012)
[26] Y S Ang, S Sultan and C Zhang, *Appl. Phys. Lett.* **97**, 243110 (2010)
[27] D S L Abergel and V I Fal'ko, *Phys. Rev. B* **75**, 155430 (2007)
[28] A R Wright, J C Cao and C Zhang, *Phys. Rev. Lett.* **103**, 207401 (2009)
[29] B Partoens and F M Peeters, *Phys. Rev. B* **75**, 193402 (2007)
[30] H Min and A MacDonald, *Phys. Rev. B* **77**, 155416 (2008)
[31] T Ohta, A Bostwick, J L McChesney, T Seyller, K Horn and E Rotenberg, *Phys. Rev. Lett.* **98**, 206802 (2007)
[32] K F Mak, J Shan and T F Heinz, *Phys. Rev. Lett.* **104**, 176404 (2010)
[33] C L Lu, C P Chang, Y C Haung, R B Chen and M L Lin, *Phys. Rev. B* **73**, 144427 (2006)
[34] I T Lin, J M Liu, K Y Shi, P S Tseng, K H Wu, C W Luo and L J Li, *Phys. Rev. B* **86**, 235446 (2012)
[35] R de Gail, M O Goerbig, F Guinea, G Montambaux and A H Castro Neto, *Phys. Rev. B* **84**, 045436 (2011)
[36] Y H Wen, Z D Chu and L Hi, *Phys. Rev. Lett.* **111**, 066803 (2013)
[37] Enamullah, Vipin Kumar, Upendra Kumar and Girish S Setlur, *Pramana – J. Phys.* **82**, 1085 (2014)
[38] M Koshino and E McCann, arXiv:1104.0794v2 (2011)
[39] F Zhang, B Sahu, H Min and A H MacDonald, *Phys. Rev. B* **82**, 035409 (2010)